Original Article

Multi-Renewable Source Integrated Microgrid System with Advanced Power Management Algorithm for Enhanced Power Distribution

Pradeep Mogilicharla[1], B. Sirisha[2], J. Upendar[3]

[1,2,3]*Department of Electrical Engineering, University College of Engineering(A), Osmania University, Telangana, India.*

[1]*Corresponding Author : pradeep.mrtgpower@gmail.com*

Abstract - Integrating multiple renewable energy sources into a three-phase grid introduces complex power quality challenges that impact the loads connected to the system. The power generated from renewable sources must be optimally utilized to ensure stable voltage levels. Energy storage systems, such as batteries and SCs, are incorporated alongside these renewable sources to stabilize voltage fluctuations. For this analysis, a microgrid system is designed, incorporating a PV source, an FC, a battery pack, and an SC, all connected to the grid. Each energy source is integrated with its power circuit to facilitate power exchange or maximum power extraction at elevated voltage levels. A central intelligent PMA controls the power flow direction of each module, ensuring efficient operation. To maximize power extraction from the PV source at higher voltage levels, a Quadratic Boost Converter is employed. The battery pack and SC utilize traditional bidirectional converters to manage the charging and discharging of the energy storage elements. The FC is connected to a conventional boost converter, enabling power sharing at medium gain voltage levels. The intelligent PMA optimizes the utilization of power from the PV source and FC while managing the charging control of the energy storage systems based on power availability. The performance of the PMA is evaluated under dynamic conditions within the microgrid system. The analysis and testing are conducted using MATLAB Simulink tools, with measured graphs plotted against time as the reference. This approach ensures a comprehensive evaluation of the system's stability and efficiency under varying operational scenarios.

Keywords - Photovoltaic (PV), Fuel Cell (FC), Super Capacitor (SC), Power Management Algorithm (PMA), MATLAB, Simulink.

1. Introduction

Renewable energy sources are often regarded as unreliable in power systems due to their dependence on unpredictable natural conditions for power generation. External power circuits controlled by intelligent algorithms are employed to address this instability. The complexity escalates when these renewable sources are integrated into the grid, as they must be synchronized with grid voltages to facilitate power injection [1]. Today's most promising renewable energy sources are photovoltaic (PV) arrays, wind farms, biogas plants, tidal energy systems, and fuel cell (FC) stations. PV arrays stand out as the most flexible and low-risk option, capable of being installed in densely populated urban areas [2]. PV panels can be mounted on building rooftops, generating solar power to meet local load demands with minimal power loss. However, since the power and voltage output of PV panels is inherently unstable, energy storage systems such as batteries and Supercapacitors (SCs) are connected in parallel to stabilize the system through power exchange [3].

In addition to these components, an FC source is integrated into the system to provide controlled renewable power generation during extreme conditions. The FC serves as a backup to both the PV source and the grid, ensuring critical loads are supported during emergencies or high-demand periods [4]. Each energy source is connected to its own power circuit, which stabilizes the DC voltage and facilitates power exchange at a common DC link [5]. The power exchange between the renewable sources and the grid is managed by a three-phase Voltage Source Converter (VSC). The VSC, a DC/AC converter topology, operates in synchronization with grid voltages to enable power transfer between the DC and AC sides of the system [6]. A central intelligent Power Management Algorithm (PMA) controls all power circuits and the VSC, utilizing feedback signals from both the DC and AC sides of the VSC [7]. Developing and implementing PMAs in renewable energy systems come with several ethical considerations. These considerations ensure the technology is deployed responsibly, equitably, and sustainably. PMAs should be designed to ensure equitable

access to energy, particularly for underserved or remote communities. Algorithms should not disproportionately benefit wealthier regions or individuals. The cost of implementing PMA-based systems should not create financial barriers for low-income households or developing regions. PMAs often rely on large amounts of data from smart meters, IoT devices, and user behavior. Ethical practices must ensure that data collection is minimal, consensual, and anonymized where possible. PMAs should prioritize using renewable energy sources and minimize reliance on fossil fuels,

contributing to global efforts to reduce carbon emissions. PMAs should avoid biases in energy distribution, ensuring that critical services (e.g., hospitals and schools) are prioritized during energy shortages. Automating energy management through PMAs could lead to job losses in traditional energy sectors. Ethical considerations should include retraining programs and support for affected workers. The structure of the proposed microgrid system, integrating multiple renewable sources with the grid, is illustrated in Figure 1.
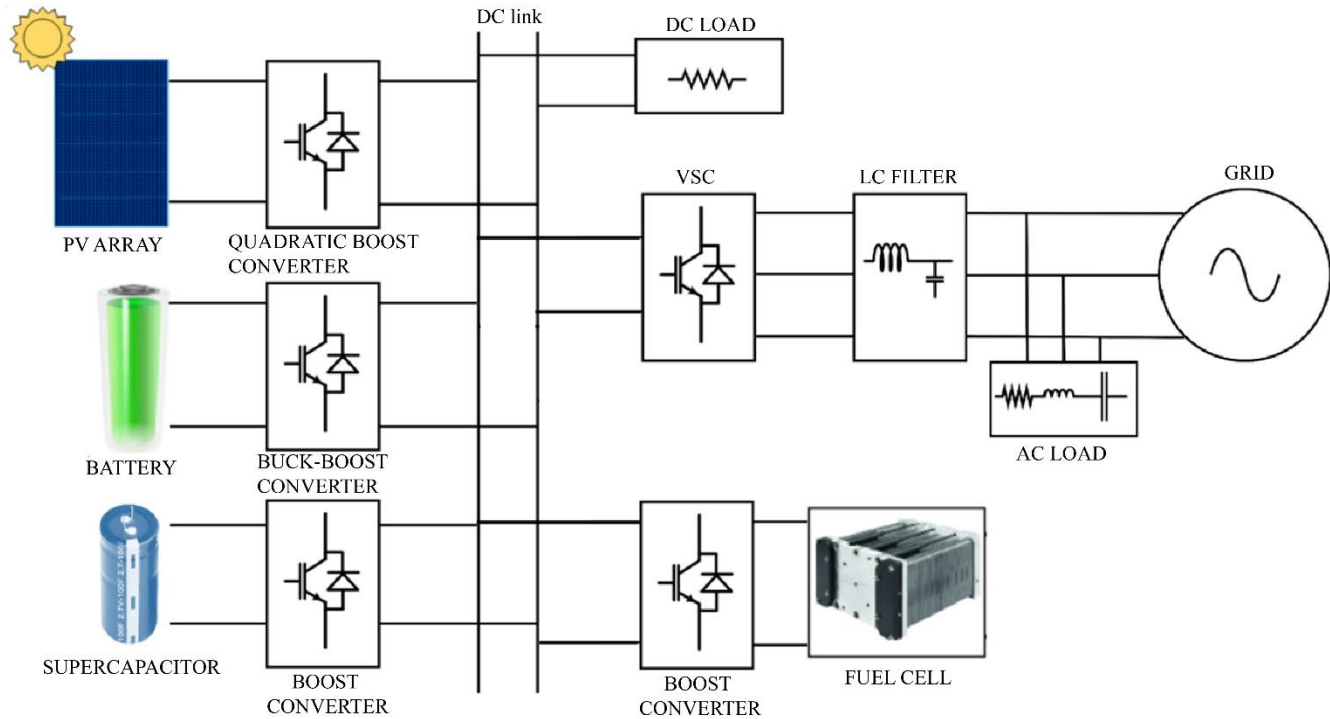

Fig. 1 Architecture of a multi-renewable source grid-integrated microgrid system

As illustrated in Figure 1, a Quadratic Boost Converter (QBC) is used to interface with the PV array, providing a high voltage gain typically in the range of 5–6 times [8]. QBCs are particularly suitable for low-voltage applications, making them an excellent choice for rooftop PV arrays with a limited number of panels connected in series, which inherently produce low voltage levels. This setup ensures efficient voltage boosting for such PV configurations.

The battery and Supercapacitor (SC) are connected via a Bidirectional Buck-Boost Converter (BD-BBC), enabling bidirectional operation for charging or discharging based on commands from the Power Management Algorithm (PMA). For the Fuel Cell (FC), a conventional Boost Converter (BC) is employed, offering a voltage amplification of 2-2.5 times. A high-gain converter is unnecessary since the FC typically operates at medium voltage levels, reducing the need for additional passive components in the converter circuit [9]. At the DC link, a Voltage Source Converter (VSC) is connected

to the grid through an LC filter to reduce harmonics caused by the switching actions of the power converter. Two types of loads-DC and AC-are supplied at the DC link and the grid's AC side, respectively. Depending on availability and demand, these loads draw power from renewable sources, energy storage systems, or the grid [10]. The Central Power Management Algorithm (PMA) determines the priority of power sources by adjusting the duty cycles of the converter switches, thereby controlling the output power of the converters. To ensure efficient load compensation, the PMA considers factors such as the State of Charge (SOC) of the energy storage systems, load power requirements, available PV generation, and grid availability. All system components are synchronized with grid voltages to optimize performance while minimizing harmonic distortion and voltage ripple.

This paper is organized as follows: Section 1 introduces the proposed multi-renewable source grid-integrated microgrid system, detailing the components and overall

system architecture. Section 2 describes the system configuration, including the circuit topologies of the integrated sources. Section 3 focuses on the Power Management Algorithm (PMA) design, covering the control structures of each power circuit, the topologies employed, and the logical framework for efficient power sharing. Section 4 presents the results and analysis of the proposed system, displaying power, voltage, and current graphs under various operating conditions to assess performance. Section 5 concludes the paper by validating the results and analyzing the system's stability and performance under specified conditions. Finally, references cited in the paper are included to support the research findings and analysis.

2. System Architecture

The proposed grid-integrated microgrid system integrates multiple renewable energy sources and energy storage elements, each controlled through dedicated circuit topologies

and individual control structures to efficiently manage power flow. Hybrid renewable energy systems, which combine diverse energy sources and storage solutions, represent an advanced approach to optimizing renewable energy generation [11]. By incorporating multiple sources, these systems improve the consistency of power generation, reducing dependence on any single energy source.

Energy storage systems play a vital role in stabilizing power delivery by addressing fluctuations in energy production. This capability ensures a smoother balance between supply and demand, facilitating the seamless integration of renewable energy into the grid while preventing disruptions [12]. Energy storage also reduces the need for fossil-fuel-based backup systems, significantly reducing greenhouse gas emissions. A detailed circuit diagram of the proposed multi-renewable source grid-integrated microgrid system is provided in Figure 2.
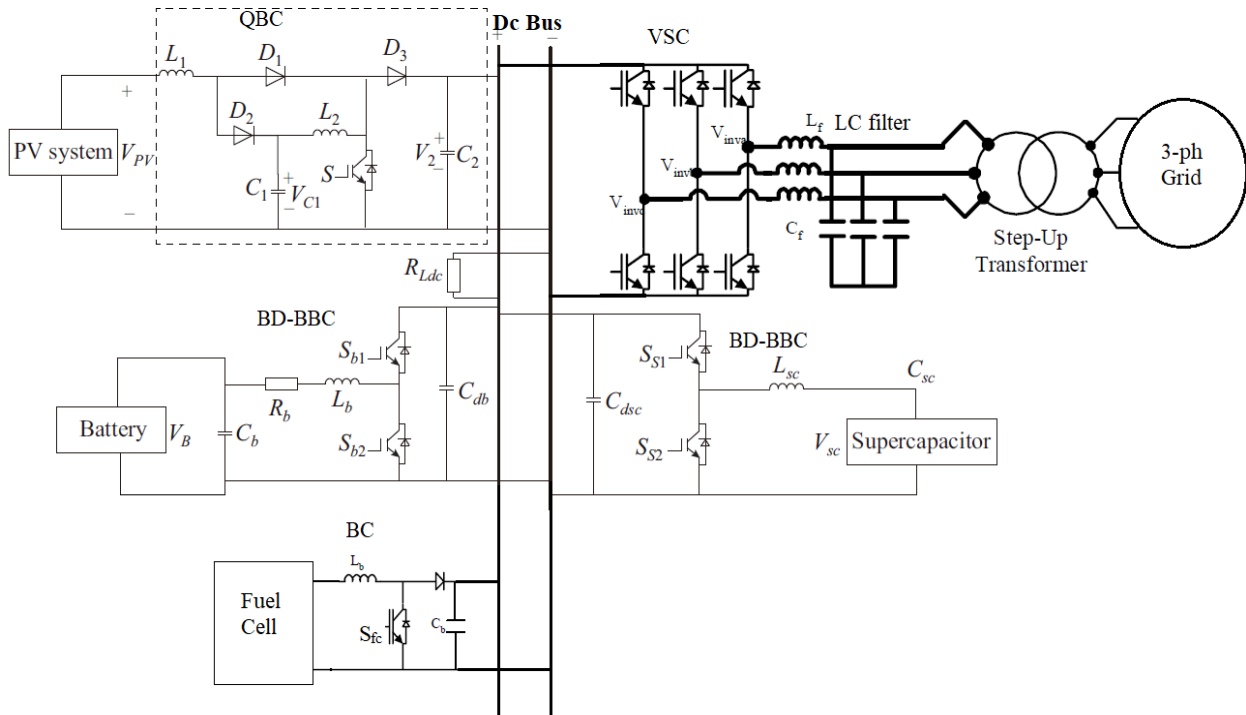

Fig. 2 Circuit configuration of the proposed system

It is noted that the Quadratic Boost Converter (QBC) for the PV source and the Boost Converter (BC) for the fuel cell (FC) each utilize a single switch (S and Sfc, respectively). In contrast, the Bidirectional Buck-Boost Converter (BD-BBC) for the battery and supercapacitor (SC) incorporates two switches. These switch pairs, Sb1-Sb2 and Ss1-Ss2, are operated alternately to prevent short circuits. The switch (S) in the PV system's QBC is controlled by an Incremental Conductance Maximum Power Point Tracking (MPPT) algorithm, which operates using the PV source's voltage and current (Vpv and Ipv) [13]. The working flow chart of the MPPT algorithm is illustrated in Figure 3.

In the presented Figure 3, the ΔV and ΔI are the change is voltage and current determined by comparing present and past values of V_{pv} and I_{pv} (V(t) I(t) and V(t-Δt) I(t-Δt)) [14]. As per these given signals, the reference PV current (I_{pvr}) is either increased or decreased by an integrated value δI expressed as:

$$I_{pvr} = I_{pv} + \int \delta I, \text{ when } \begin{cases} \frac{\Delta I}{\Delta V} \geq \frac{-I}{V} \text{ and } \Delta V \neq 0 \\ \Delta I > 0 \text{ and } \Delta V = 0 \end{cases} \quad (1)$$

$$I_{pvr} = I_{pv} - \int \delta I, \text{ when } \begin{cases} \frac{\Delta I}{\Delta V} < \frac{-I}{V} \text{ and } \Delta V \neq 0 \\ \Delta I < 0 \text{ and } \Delta V = 0 \end{cases} \quad (2)$$
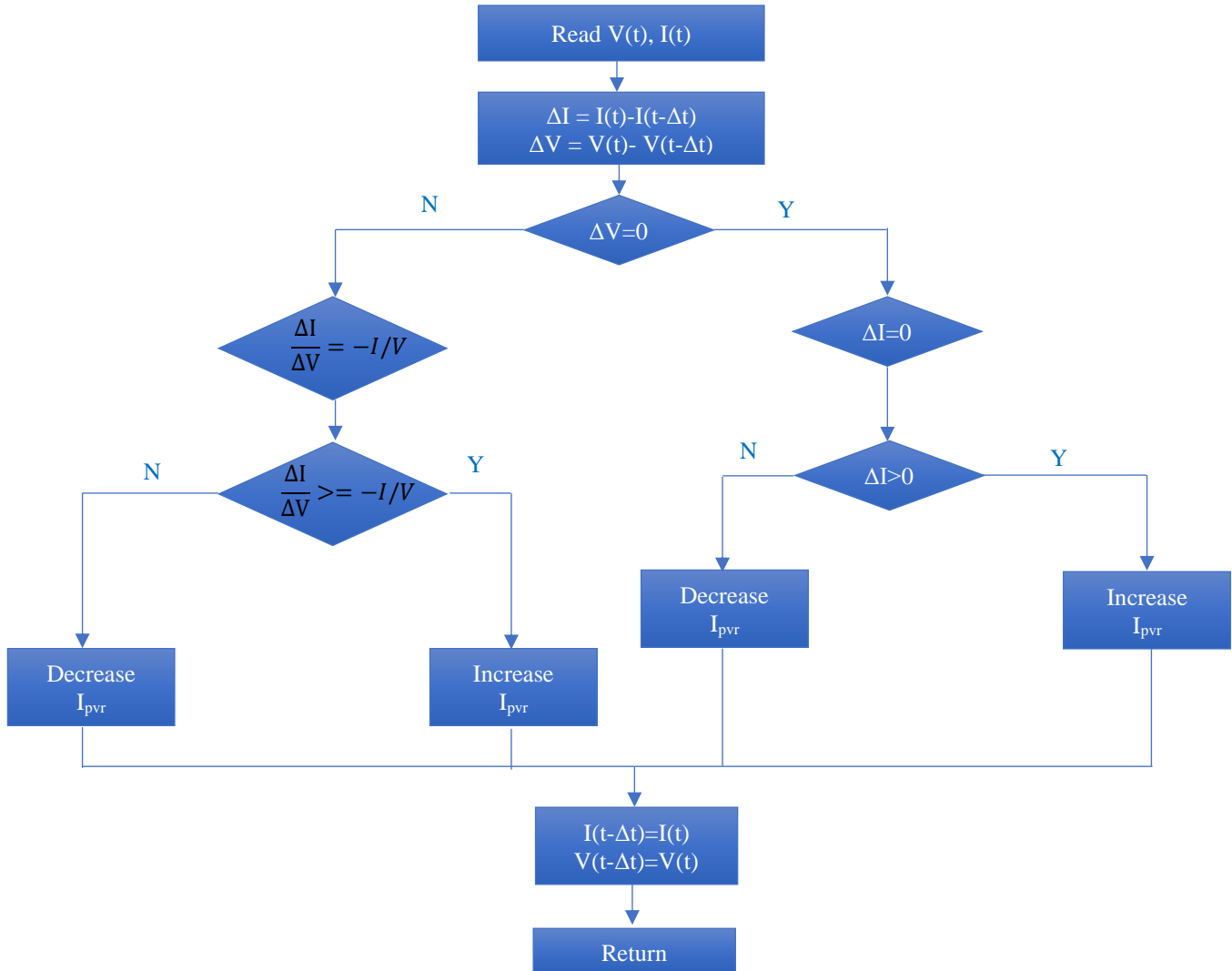
Fig. 3 Incremental conductance MPPT

From Equations (1) and (2), the reference PV current (I_pvr) is updated and compared to the measured PV current signal (Ipv) [15]. The resulting current error is sent to a current regulator (PI controller), which determines the required duty ratio for the switch (S). This duty ratio is then compared to a high-frequency sawtooth waveform generator, which produces the pulse signals to control the QBC switch. The control structure of the QBC, incorporating the MPPT algorithm and voltage regulator, is illustrated in Figure 4.

The QBC control structure operates as an independent module, ensuring maximum power extraction from the PV panels regardless of grid conditions. The Power Management Algorithm (PMA) is not integrated into the QBC control because the power from the PV source is consistently extracted and delivered to either the grid, loads, or energy storage systems. Instead, the PMA controls the switches of the Bidirectional Buck-Boost Converters (BD-BBCs) and the Boost Converter (BC) for the battery, Supercapacitor (SC), and Fuel Cell (FC) modules.
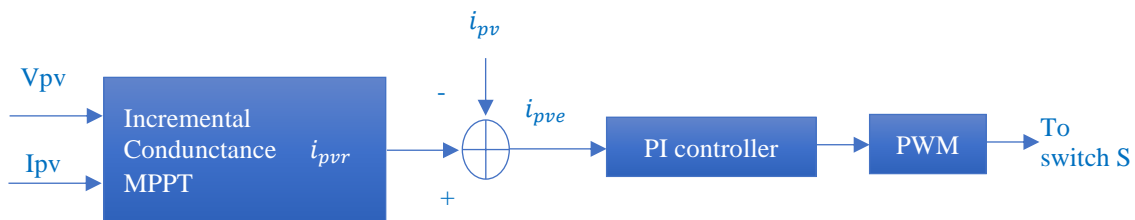

Fig. 4 QBC control structure

For the bidirectional operation of the Voltage Source Converter (VSC), a Synchronous Reference Frame (SRF) method is implemented, incorporating current and voltage regulators to ensure stability [16]. The SRF control for the VSC uses feedback from the inverter currents and grid voltages to manage power sharing between the DC and AC sides in synchronization. The reference dq signals for the VSC control are defined as follows:

$$V_{d-ref} = Ud + Vd + L\omega I_q \qquad (3)$$

$$V_{q-ref} = Uq + Vq - L\omega I_d \qquad (4)$$

Here, $Vd \ Vq$ are the measured grid voltage dq components, L is the filter inductance value, ω is the angular frequency of the grid ($2\pi f$), $I_d I_q$ are the measured inverter current dq components and $Ud \ Uq$ are determined as:

$$Ud = (i_{d-ref} - i_d)\left(K_{pi} + \frac{K_{ii}}{s}\right) \qquad (5)$$

$$Uq = (i_{q-ref} - i_q)\left(K_{pi} + \frac{K_{ii}}{s}\right) \qquad (6)$$

Here, Kpi and Kii represent the proportional and integral gains of the current regulator, respectively. The quadrature-axis reference current *iq-ref* is set to zero to ensure no reactive power exchange from the VSC, while the direct-axis reference current *id-ref* is adjusted according to the load demand. The dq components from equations (3) and (4) are converted into reference sinusoidal signals (*Vabc-ref*) using Inverse Park's Transformation [17]. The measured *Vq*, *Id*, and *Iq* components are generated through Park's Transformation. Finally, the *Vabc-ref* signals are compared with a high-frequency triangular carrier wave to generate the switching pulses for the VSC.

3. PMA Design

As mentioned earlier, the PMA controls the switches of the BD-BBCs connected to the energy storage elements (battery and SC), and the BC is linked to the FC source. The PMA receives feedback signals from the PV source power (*Ppv*), the SOC of the battery and SC (*SOCb* and *SOCsc*), the DC link voltage (*Vdc*), and the load demand power (*PL*). Based on these inputs, the PMA generates reference current signals to regulate the power flow of the battery, SC, and FC. These reference current signals control the converter switches through current regulators (PI controllers) and PWM generators. The complete structure of the PMA for the proposed multi-renewable source grid-integrated microgrid system is illustrated in Figure 5.
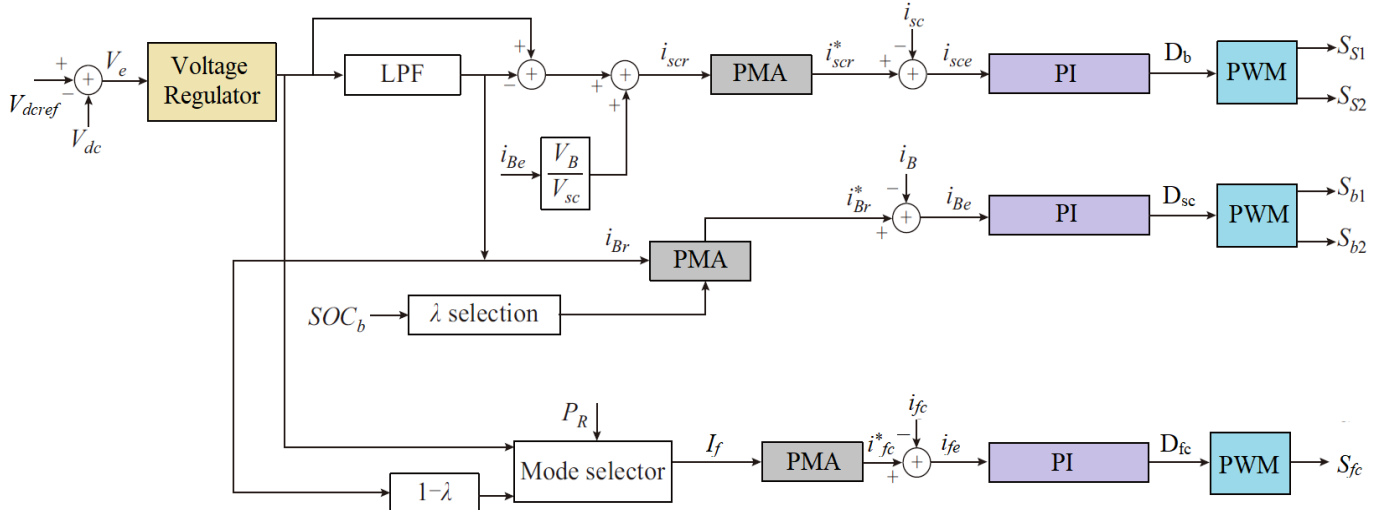

Fig. 5 PMA structure for converters control

As presented in Figure 5, the PMA generates the reference current signals (i^*_{scr}, i^*_{Br} *and* i^*_{fc}) for controlling the converter switches with the duty ratio signals (D_b, D_{sc} and D_{fc}). All these duty ratio signals are generated by individual current PI controllers [18]. The reference current signals are generated per the SOC_b and SOC_{sc} measured at the battery and SC elements. As per the PV power generation, the system operates in three modes mentioned: a) DPM (Deficit Power Mode), b) EPM (Excess Power Mode) and c) BPM (Balanced Power Mode) [19]. The DPM occurs when $P_{pv} > P_L$, EPM occurs during $P_{pv} < P_L$ and BPM occurs at $P_{pv} = P_L$ [20]. As per these modes, the reference current signals are generated with respect to Table 1.

Table 1. Reference current signals generation of PMA

DPM	
SOC Range	Reference Currents
$SOC_b > L$; $SOC_{sc} > L$	$i^*_{Br} = \lambda i^*_y$; $i^*_{scr} = i'_y$; $i^*_{fc} = (1-\lambda)i^*_y$
$SOC_b < L$; $SOC_{sc} > L$	$i^*_{Br} = 0$; $i^*_{scr} = i'_y$; $i^*_{fc} = i^*_y$
$SOC_b > L$; $SOC_{sc} < L$	$i^*_{Br} = \lambda i^*_y$; $i^*_{scr} = 0$;

SOC range	Reference currents
	$i_{fc}^* = (1-\lambda)i_y$
$SOC_b < L$; $SOC_{sc} < L$	$i_{Br}^* = 0$; $i_{scr}^* = 0$; $i_{fc}^* = i_y$
EPM	
SOC range	Reference currents
$SOC_b < U$; $SOC_{sc} < U$	$i_{Br}^* = i_{B.ch}$; $i_{scr}^* = i_{SC.ch}$; $i_{fc}^* = i_y$
$SOC_b < U$; $SOC_{sc} > U$	$i_{Br}^* = i_{B.ch}$; $i_{scr}^* = i_y'$; $i_{fc}^* = i_y - i_{scr}$
$SOC_b > U$; $SOC_{sc} < U$	$i_{Br}^* = 0$; $i_{scr}^* = i_{SC.ch}$; $i_{fc}^* = i_y$
$SOC_b > U$; $SOC_{sc} > U$	$i_{Br}^* = 0$; $i_{scr}^* = i_y'$; $i_{fc}^* = 0$
BPM	
SOC range	Reference currents
$SOC_b < U$; $SOC_{sc} < U$	$i_{Br}^* = i_{B.ch}$; $i_{scr}^* = i_{SC.ch}$; $i_{fc}^* = i_{Br}^* + i_{scr}^*$
$SOC_b < U$; $SOC_{sc} > U$	$i_{Br}^* = i_{B.ch}$; $i_{scr}^* = i_y'$; $i_{fc}^* = i_{Br}^*$
$SOC_b > U$; $SOC_{sc} < U$	$i_{Br}^* = 0$; $i_{scr}^* = i_{SC.ch}$; $i_{fc}^* = i_{scr}^*$
$SOC_b > U$; $SOC_{sc} > U$	$i_{Br}^* = 0$; $i_{scr}^* = i_y'$; $i_{fc}^* = 0$

Table 2. λ value selection

SOC_b	λ
$0.8 < SOC_b < 0.95$	1
$0.45 < SOC_b < 0.8$	0.6
$0.15 < SOC_b < 0.45$	0.3
$SOC_b < 0.15$	0

In the given reference current generation concerning the mode, the λ value is selected as per the SOC_b provided in Table 2. In Table 2, the SOC is represented in perunit (80% = 0.8).

The λ value selected from the SOC_b, the reference current magnitude varies [21] [22]. The values of the currents in Table 1 are generated by DC link voltage (V_{dc}) comparison with a reference value ($V_{dc\,ref}$).

$$i_y = (V_{dc\,ref} - V_{dc})(K_p + \int K_i) \tag{7}$$

$$i_y^* = \frac{w_c}{s+w_c} i_y \tag{8}$$

$$i_y' = \left(1 - \frac{w_c}{s+w_c}\right) i_y \tag{9}$$

Here, $K_p K_i$ are the voltage regulator proportional and integral gains, w_c is the filter cut-off frequency; during the charging modes of the battery and SC, the currents are given as:

$$i_{B.ch} = \frac{-P_{Br}}{V_B} \tag{10}$$

$$i_{SC.ch} = -P_{sc}\sqrt{\frac{C_{sc}}{2E_{sc}}} \tag{11}$$

Here, V_B and P_{Br} are the voltage and maximum charge power of the battery, C_{sc} E_{sc} and P_{sc} are the capacity, energy and maximum charge power of the SC [23]. The charge current values are negative, which represents the charging of the elements. The performance of the PMA is analysed using different operating conditions, and all modes are observed in the following section.

4. Simulation Analysis and Results Discussion

The modeling of the proposed multi-renewable source grid-integrated microgrid system is developed in the Simulink environment of MATLAB software. Electrical components are selected from the 'Simpowersystems' library subset, while control design blocks are taken from the 'Commonly Used Blocks subset of the Simulink library. The system model is analyzed using discrete analysis with the 'Tustin' solver selected in the 'powergui' settings. To ensure detailed and accurate graph generation, a sampling time of 1 μsec is configured for the analysis. The model is updated with the parameters provided in Table 3, which are chosen based on standard system configurations.

Table 3. System parameters

Name of the Unit	Parameters
Grid	132kV, 50Hz, 2500MVA, X/R = 7
PV panels	V_{mp} = 41.5V, I_{mp} = 8.07A, V_{oc} = 49.9V, I_{sc} = 9A, N_s = 9, N_p = 7, P_{pv} = 21kW QBC: $L_1 = L_2$ = 1mH, $C_1 = C_2$ = 100μF
PEMFC	V_{nom} = 400V, I_{nom} = 80A, V_{end} = 166V, I_{end} = 280A BC: L_{b2} = 1mH, C_{in} = 100μF
BES	V_{nom} = 400V, Capacity = 100Ahr BD-BBC: L_{bb1} = 1mH, R_{igbt} = 1mΩ
SC	V_{rated} = 400V, C_{sc} = 3F, R_{sc} = 8.9mΩ, N_s = 18, N_p = 1 BD-BBC: L_{bb1} = 1mH, R_{igbt} = 1mΩ
VSC	R_{igbt} = 1mΩ, V_{dcref} = 750V, f_s = 5kHz SRF: K_{pi} = 0.3, K_{ii} = 20, V_{dcref} = 750V.
Load	Static load = 10kW, Dynamic load = 40kW

Using the parameters specified in Table 3, the model is simulated for 4 seconds under variable solar irradiation and dynamic load conditions. Graphs of various parameters from the integrated modules are plotted against time in the figures below. The solar irradiation is initially set at its optimum level

of 1000 W/m², which is then reduced to half (500 W/m²) at the 1-second mark. A dynamic load is introduced into the system only between 2 and 3 seconds of the simulation. This increases the load demand from 10 kW to 50 kW during this interval,

affecting the power sources connected to the system. The characteristics of all modules, along with the power exchange dynamics under the given solar irradiation and load demand conditions, are presented in the results.
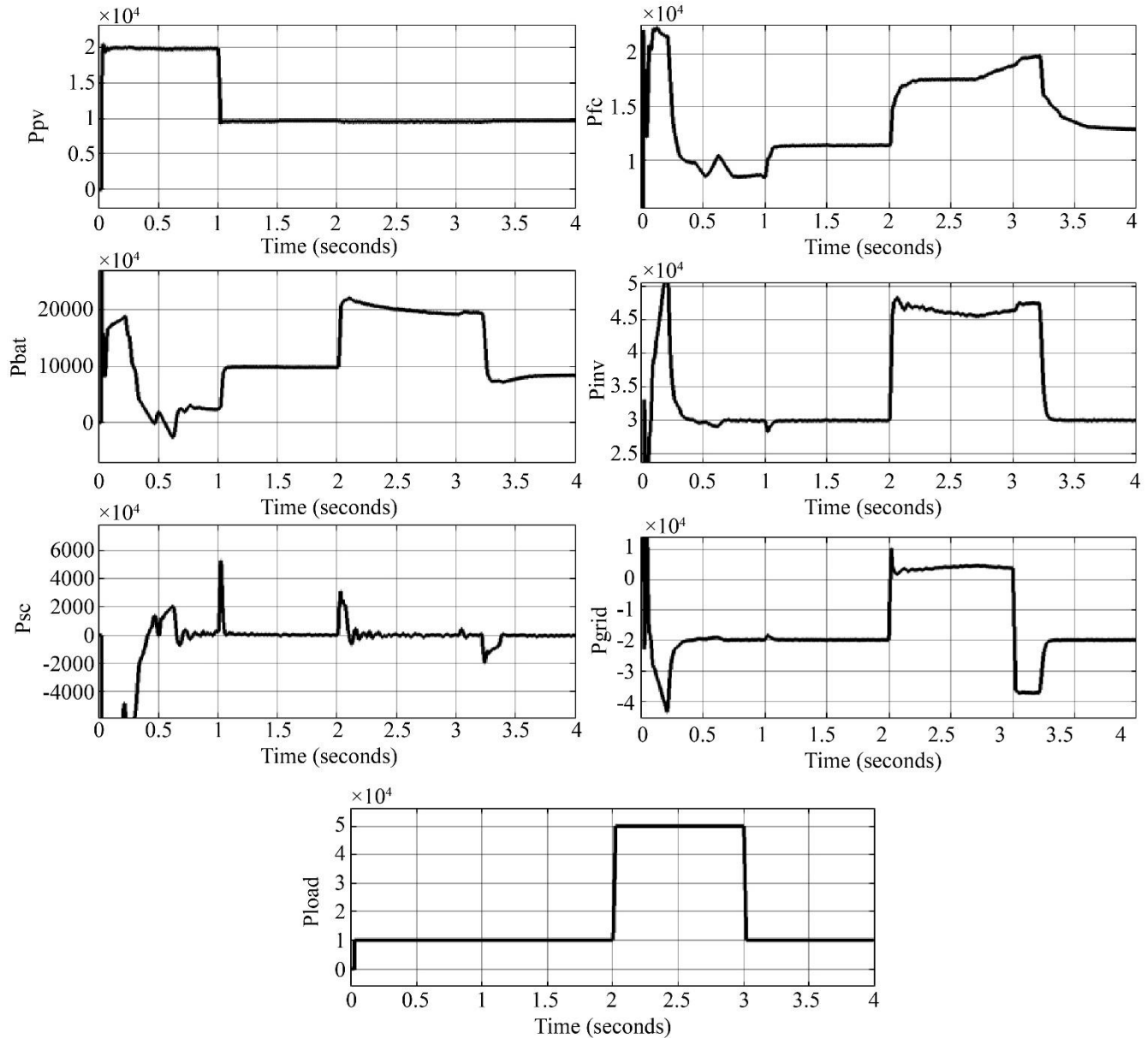

Fig. 6 Active powers of all modules

Figure 6 illustrates the active powers of all source modules, which vary according to the conditions defined in the model. As the solar irradiation decreases from 1000 W/m² to 500 W/m² at the 1-second mark, the PV power drops from 20 kW to 10 kW, with maximum power extraction maintained by the MPPT-controlled QBC. Immediately following this drop, the power from the battery and FC increases from 5 kW to 10 kW each. During the period from 0 to 2 seconds, the total power delivered by the VSC to the grid remains constant at 30

kW despite the change in solar irradiation. Of this 30 kW, 10 kW is consumed by the static load, while the remaining 20 kW is injected into the grid.

At the 2-second mark, when the dynamic load increases by 40 kW, the total load demand rises to 50 kW. This surge in demand leads to increased power extraction from the battery and FC. The battery power rises from 10 kW to 20 kW, and the FC power increases from 10 kW to 17 kW. Consequently,

the total power delivered by the VSC reaches 45 kW (after accounting for 2 kW of conversion losses). The remaining 5 kW required to meet the 50kW load demand is drawn from the grid. Once the dynamic load is removed and the system reverts to the 10kW static load, all power values return to their previous levels. It is observed that the SC power briefly spikes to provide instantaneous compensation during dynamic load changes. The SC continuously charges and discharges, supplying necessary power to the system during sudden variations, ensuring stability and efficient power management.
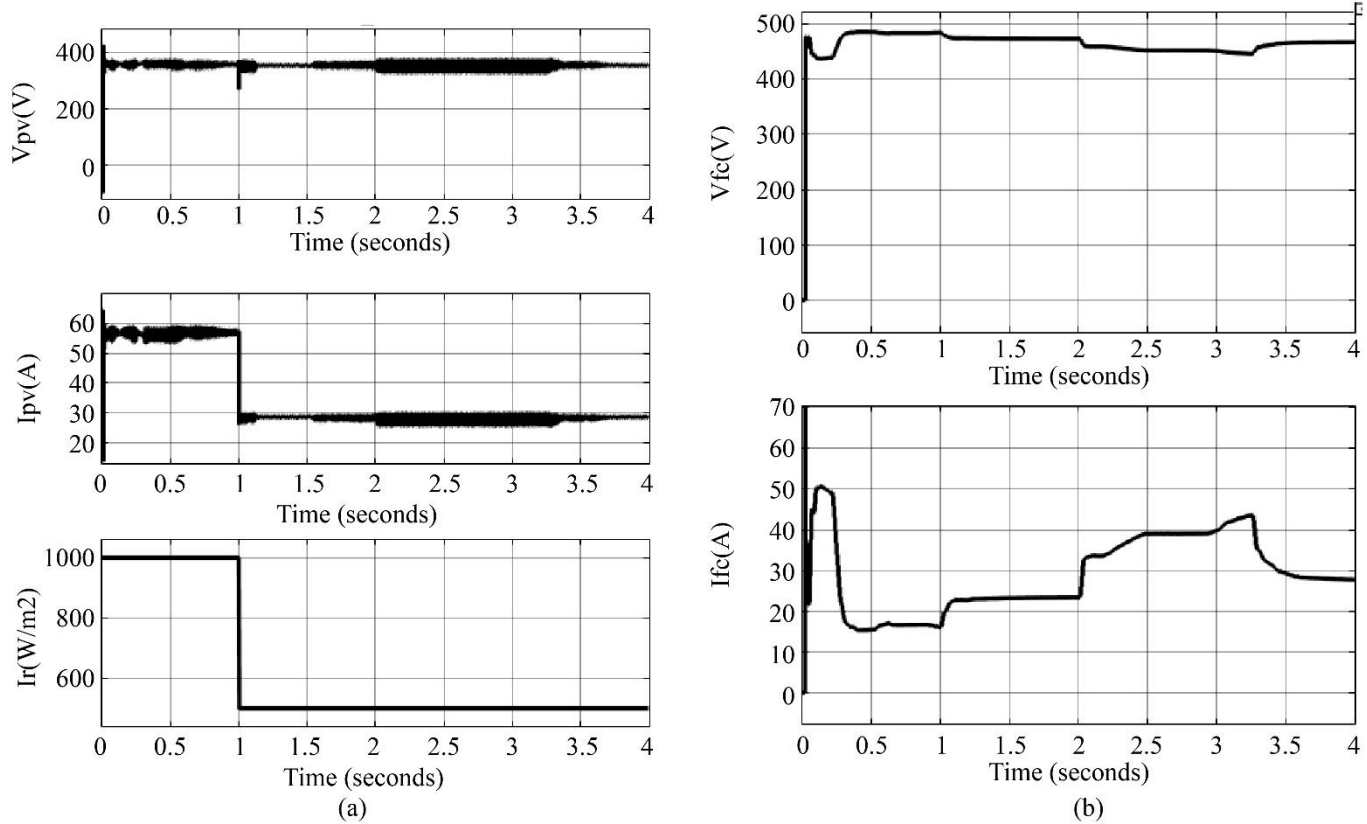

Fig. 7 Characteristics of (a) PV array, and (b) FC

Figures 7(a) and 7(b) depict the characteristics of the PV and FC modules, highlighting the variations in their currents in response to changes in the system. The PV and FC voltages remain close to 400 V throughout the simulation, with an acceptable ripple level. However, the PV current drops by half when the solar irradiation is reduced by 50%. On the other hand, the FC current shows a slight increase when the irradiation decreases but doubles when the load demand rises significantly. These variations demonstrate the dynamic response of the system to changing conditions.

Figures 8(a) and 8(b) illustrate the characteristics of the energy storage elements, the battery and the supercapacitor (SC), respectively. The battery voltage is maintained at 400 V, while the SC voltage remains at 300 V. The battery current increases gradually when the solar irradiation drops and eventually doubles when the load demand on the AC side rises.

The SC current exhibits spikes in both positive and negative directions, indicating rapid charging and discharging

in response to dynamic system conditions. As the battery continuously discharges throughout the simulation, its State of Charge (SOCb) steadily declines. In contrast, the SOC of the SC (SOCsc) is maintained at 80%, ensuring it can provide immediate support to the system during sudden variations.

Figures 9(a) and 9(b) depict the DC link voltage, as well as the three-phase voltages and currents of the Voltage Source Converter (VSC) after the step-up transformer. The DC link voltage remains stable at approximately 750 V, with only a negligible drop observed. The AC voltages and currents exhibit minimal harmonic distortion, thanks to the effective mitigation provided by the LC filter connected after the VSC.

Figure 10 shows graphs of reference currents generated by the PMA based on the changes set in the simulation model. The i^*_{sc} is averagely maintained at zero, with small overshoots during the variations. The i^*_{bat} and i^*_{fc} reference currents vary as per changes in the solar irradiation and load demand. It is observed that the i^*_{fc} signal is always on the positive side as the FC is not a storage device.
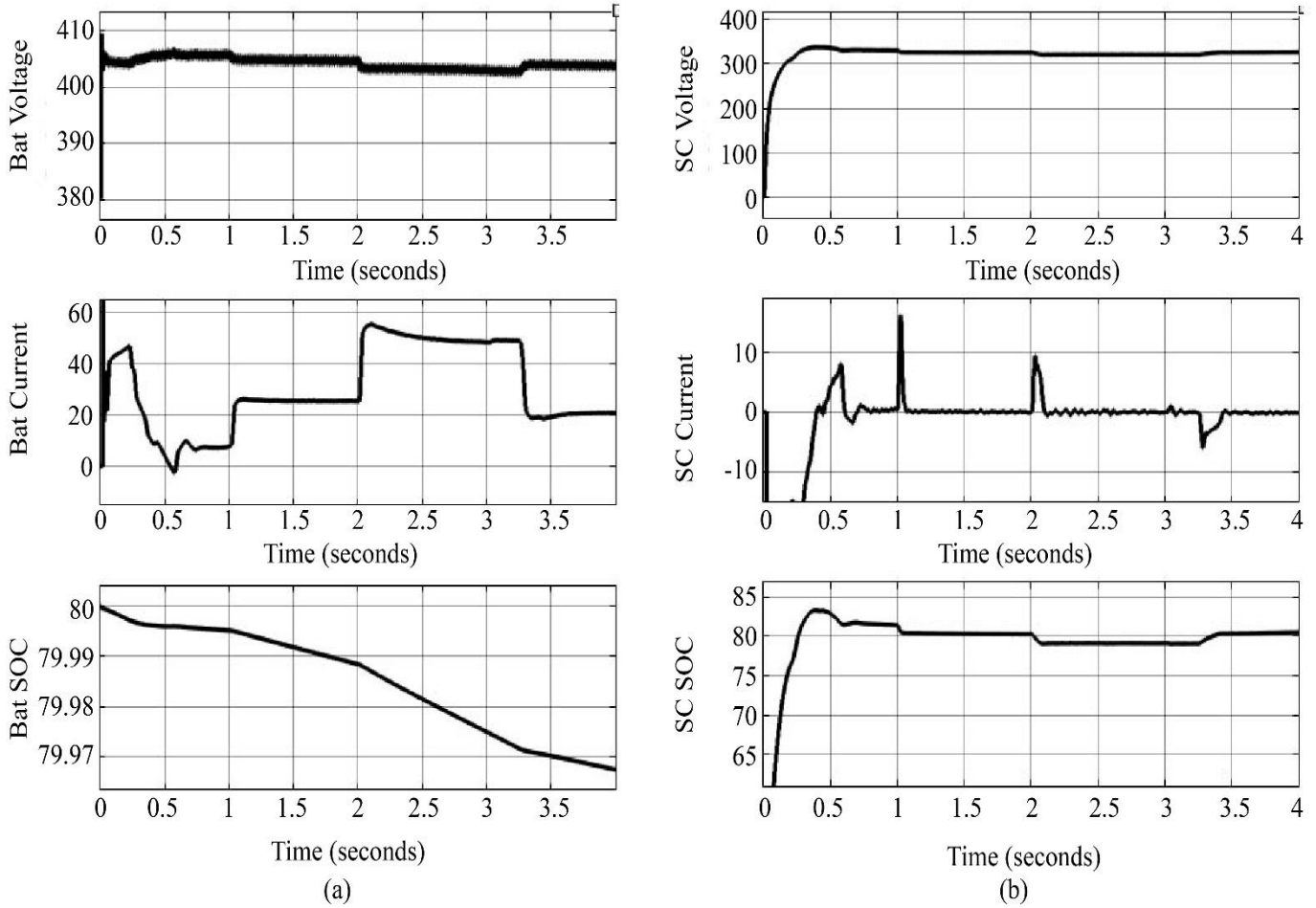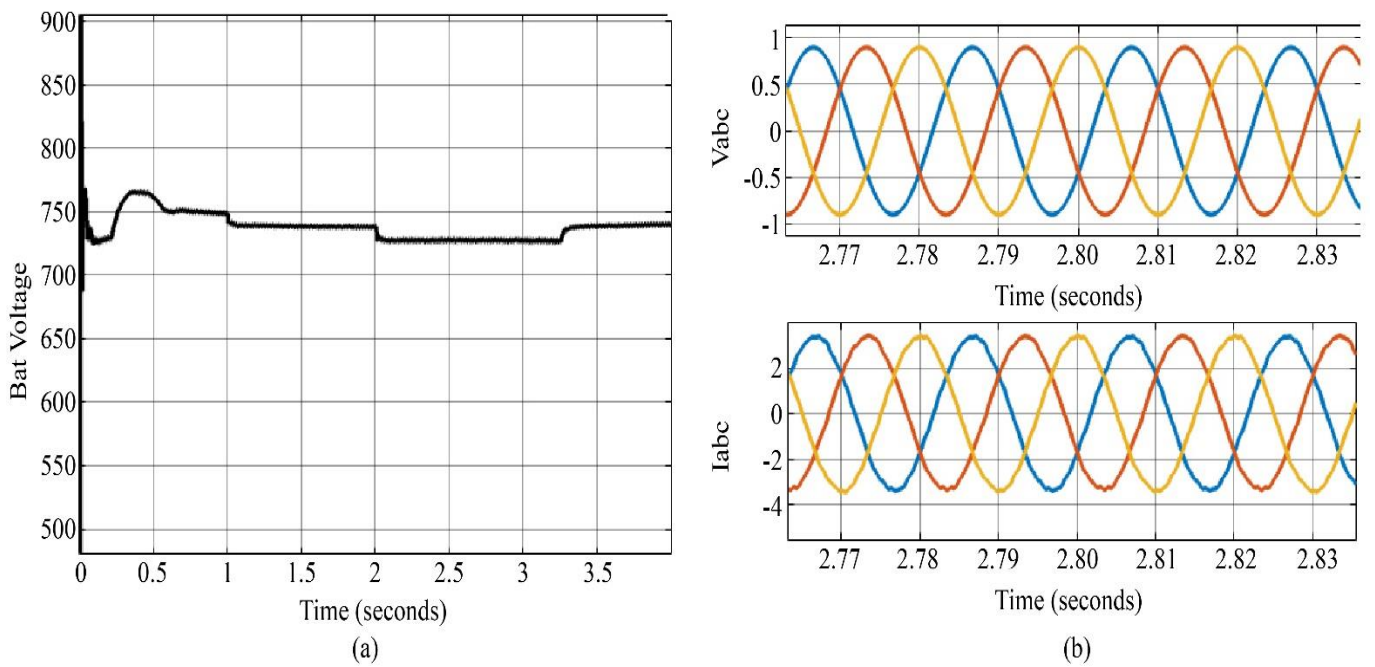
Fig. 8 Characteristics of (a) Battery, and (b) SC

Fig. 9 (a) DC link voltage, and (b) Three phase voltages and current of the VSC
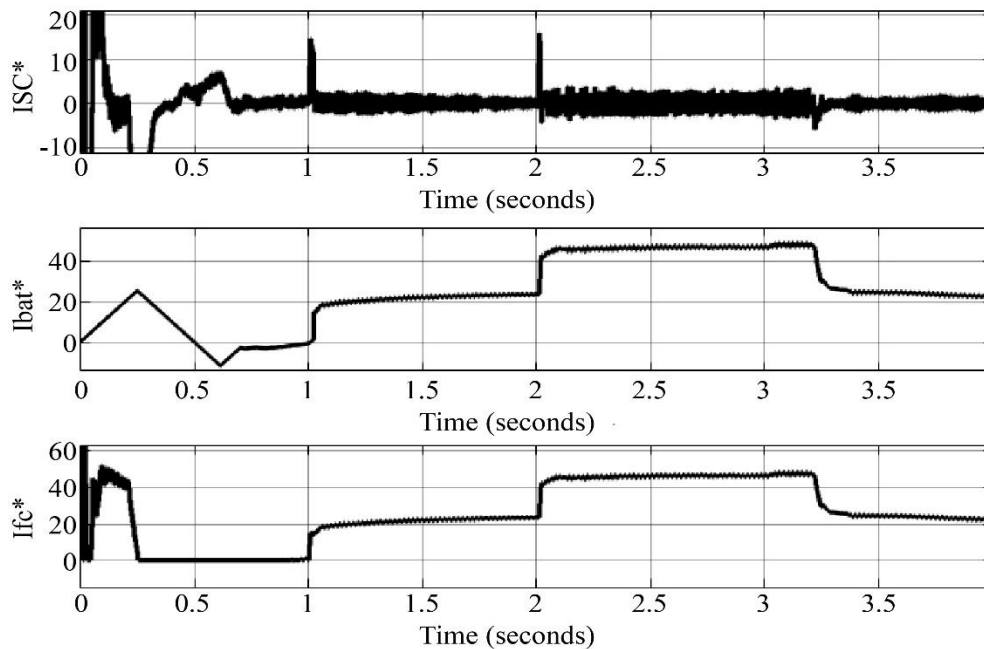
Fig. 10 Reference currents generated by the PMA

5. Conclusion

In the proposed model, hybrid renewable sources, such as PV and FC, are integrated with the grid to deliver renewable power and support the load. These renewable sources are stabilized using energy storage systems, including batteries and SC, providing sustained and instantaneous backup. The battery stores higher energy levels, while the SC delivers rapid power bursts, shielding the battery from sudden current fluctuations. Maximum power extraction from the PV panels is ensured through a QBC controlled by the Incremental Conductance MPPT algorithm. The BD-BBC for the battery and SC, along with the BC for the FC, are regulated by a central PMA to optimize power distribution and meet load demands. The PMA prioritizes using renewable energy, reducing dependence on conventional grid power. The results indicate that grid power compensation is minimal, with renewable power predominantly meeting demand during low-load conditions. PV, battery, and FC-generated power are either fed into the grid or supplied to the load through an SRF-controlled VSC.

The PMA's performance is demonstrated to be highly efficient, showcasing the system's robustness in handling sudden changes in load or renewable power availability. The number of renewable sources in the system can be increased with further modification of the system. The PMA can be updated with an advanced and adaptive controller for better control over the voltage, resulting in lower harmonic levels.

References

[1] Praveen Tiwari et al., "A Review on Microgrid Based on Hybrid Renewable Energy Sources in South-Asian Perspective," *Technology and Economics of Smart Grids and Sustainable Energy*, vol. 2, no. 1, pp. 1-16, 2017. [CrossRef] [Google Scholar] [Publisher Link]

[2] Anushika Bandara, KTMU Hemapala, and Nalin C. Ekanayake, "A Survey on Hybrid Renewable Energy Systems for Microgrid Application," *2020 IEEE 9th Power India International Conference*, Sonepat, India, pp. 1-6, 2020. [CrossRef] [Google Scholar] [Publisher Link]

[3] Asmita Ajay Rathod, and Balaji Subramanian, "Scrutiny of Hybrid Renewable Energy Systems for Control, Power Management, Optimization and Sizing: Challenges and Future Possibilities," *Sustainability*, vol. 14, no. 24, pp. 1-35, 2022. [CrossRef] [Google Scholar] [Publisher Link]

[4] V.V.S.N. Murty, and Ashwani Kumar, "Multi-Objective Energy Management in Microgrids with Hybrid Energy Sources and Battery Energy Storage Systems," *Protection and Control of Modern Power Systems*, vol. 5, no. 1, pp. 1-20, 2020. [CrossRef] [Google Scholar] [Publisher Link]

[5] Anindya Bharatee, Pravat K. Ray, and Arnab Ghosh, "A Power Management Scheme for Grid-Connected PV Integrated with Hybrid Energy Storage System," *Journal of Modern Power Systems and Clean Energy*, vol. 10, no. 4, pp. 954-963, 2022. [CrossRef] [Google Scholar] [Publisher Link]

[6] Chitra Natesan et al., "Power Management Strategies in Microgrid: A Survey," *International Journal of Renewable Energy Research*, vol. 5, no. 2, pp. 334-340, 2015. [Google Scholar] [Publisher Link]

[7] Zhehan Yi, Wanxin Dong, and Amir H. Etemadi, "A Unified Control and Power Management Scheme for PV-Battery-Based Hybrid Microgrids for Both Grid-Connected and Islanded Modes," *IEEE Transactions on Smart Grid*, vol. 9, no. 6, pp. 5975-5985, 2018. [CrossRef] [Google Scholar] [Publisher Link]

[8] Jianfang Xiao, Peng Wang, and Leonardy Setyawan, "Multilevel Energy Management System for Hybridization of Energy Storages in DC Microgrids," *IEEE Transactions on Smart Grid*, vol. 7, no. 2, pp. 847-856, 2016. [CrossRef] [Google Scholar] [Publisher Link]

[9] Jing Yang et al., "An Improved Artificial Ecosystem-Based Optimization Algorithm for Optimal Design of a Hybrid Photovoltaic/Fuel Cell Energy System to Supply a Residential Complex Demand: A Case Study for Kuala Lumpur," *Energies*, vol. 16, no. 6, pp. 1-21, 2023. [CrossRef] [Google Scholar] [Publisher Link]

[10] Yunjie Gu et al., "Mode-Adaptive Decentralized Control for Renewable Dc Microgrid with Enhanced Reliability and Flexibility," *IEEE Transactions on Power Electronics*, vol. 29, no. 9, pp. 5072-5080, 2014. [CrossRef] [Google Scholar] [Publisher Link]

[11] Narsa Reddy Tummuru, Mahesh K. Mishra, and S. Srinivas, "Dynamic Energy Management of Renewable Grid Integrated Hybrid Energy Storage System," *IEEE Transactions on Industrial Electronics*, vol. 62, no. 12, pp. 7728-7737, 2015. [CrossRef] [Google Scholar] [Publisher Link]

[12] Bhim Singh, D.T Shahani, and Aran Kumar Verma, "IRPT Based Control of A 50 Kw Grid Interfaced Solar Photovoltaic Power Generating System with Power Quality Improvement," *2013 4th IEEE International Symposium on Power Electronics for Distributed Generation Systems*, Rogers, AR, USA, pp. 1-8, 2013. [CrossRef] [Google Scholar] [Publisher Link]

[13] Necmi Altin, and Ertan Ozturk, "Maximum Power Point Tracking Quadratic Boost Converter for Photovoltaic Systems," *2016 8th International Conference on Electronics, Computers and Artificial Intelligence*, Ploiesti, Romania, pp. 1-4, 2016. [CrossRef] [Google Scholar] [Publisher Link]

[14] Salheddine Belhimer, Mourad Haddadi, and Adel Mellit, "Design of a Quadratic Boost Converter for a Standalone PV System Based on INC MPPT Algorithm," *Proceedings of the 1st International Conference on Electronic Engineering and Renewable Energy*, Saidia, Morocco, pp. 447-453, 2018. [CrossRef] [Google Scholar] [Publisher Link]

[15] Praveen Kumar Mishra, and Prabhakar Tiwari, "Incremental Conductance MPPT in Grid Connected PV System," *International Journal of Engineering, Science and Technology*, vol. 13, no. 1, pp. 138-145, 2021. [CrossRef] [Google Scholar] [Publisher Link]

[16] T. Sathiyanarayanan, and S. Mishra, "Synchronous Reference Frame Theory Based Model Predictive Control for Grid Connected Photovoltaic Systems," *IFAC-PapersOnLine*, vol. 49, no. 1, pp. 766-771, 2016. [CrossRef] [Google Scholar] [Publisher Link]

[17] V. Sowmya Sree, G. Panduranga Reddy, and C. Srinivasa Rao, "Mitigation of Power Quality Issues in Hybrid Solar-Wind Energy System Using Distributed Power Flow Controller," *2021 IEEE International Women in Engineering (WIE) Conference on Electrical and Computer Engineering*, Dhaka, Bangladesh, pp. 162-166, 2021. [CrossRef] [Google Scholar] [Publisher Link]

[18] Elizabeth Noghreian, and Hamid Reza Koofigar, "Power Control of Hybrid Energy Systems with Renewable Sources (Wind-Photovoltaic) Using Switched Systems Strategy," *Sustainable Energy, Grids and Networks*, vol. 21, 2020. [CrossRef] [Google Scholar] [Publisher Link]

[19] Djamila Rekioua et al., "Power Management Control of an Autonomous Photovoltaic/Wind Turbine/Battery System," *Energies*, vol. 16, no. 5, pp. 1-24, 2023. [CrossRef] [Google Scholar] [Publisher Link]

[20] V. Mounica, and Y.P. Obulesu, "Hybrid Power Management Strategy with Fuel Cell, Battery, and Supercapacitor for Fuel Economy in Hybrid Electric Vehicle Application," *Energies*, vol. 15, no. 2, pp. 1-25, 2022. [CrossRef] [Google Scholar] [Publisher Link]

[21] Z. Sabiri et al., "A New Architecture of Energy Management Applied to Hybrid Renewable Energy System," *2017 29th International Conference on Microelectronics*, Beirut, Lebanon, pp. 1-4, 2017. [CrossRef] [Google Scholar] [Publisher Link]

[22] N.S. Jayalakshmi, D.N. Gaonkar, and Pramod Bhat Nempu, "Power Control of PV/Fuel Cell/Supercapacitor Hybrid System for Stand-Alone Applications," *International Journal of Renewable Energy Research*, vol. 6, no. 2, pp. 672-679, 2016. [CrossRef] [Google Scholar] [Publisher Link]

[23] Nassereddine Dahmane et al., "Energy Management of PV/FC/BAT/SC and PEM Electrolyzer," *2022 IEEE International Conference on Electrical Sciences and Technologies in Maghreb*, Tunis, Tunisia, pp. 1-6, 2022. [CrossRef] [Google Scholar] [Publisher Link]